VCST Internal Memo

Title: Analysis of FP-10 Part 2 Thermal Band Response Versus Scan Angle Determination
Memo Number: 2014_018
Revision: 01
Date: August 15, 2014
Author: Jeff McIntire
To: Xiaoxiong Xiong and James Butler
Cc: Hassan Oudrari, Kwo-Fu (Vincent) Chiang, Jon Fulbright and Aisheng Wu

References

[1] TP1544640-2221 Rev A, 'Response Versus Scan Angle Test FP-10,' Raytheon.
[2] VCST_TECH_REPORT_14_008, 'Preliminary Analysis of FP-10 Part 2,' Jeff McIntire, January 14, 2014.
[3] NICST_MEMO_10_026, 'Updated Analysis Results in the VIIRS FU1 Response Versus Scan Angle (RVS) for FP-10 TEB,' Jeff Cronkhite and Jeff McIntire, October 8, 2010.
[4] Y18352, 'Performance Verification Review: Thermal Emissive Band Radiometric response Characterization (RC-3 and RC-5 Tests),' Eric Johnson and Jim Young, January 18, 2006.
[5] NICST_MEMO_11_001, 'Analysis of the Radiometric Calibration from the VIIRS F1 RC-05 Part 1 Test (Nominal Plateau, Electronic Side B),' Jeff McIntire and Sanxiong Xiong, January 3, 2011.

1. Introduction

The VIIRS F2 test FP-10 part 2 was designed to determine the response versus scan angle (RVS) for the thermal bands [1]. Preliminary analysis was reported in [2], based on the methodology adopted in [3].

Tables 1 and 2 list the UAIDs, collects, LABB scan angle and HAM AOI, sample numbers used, collect window, and LABB and OBC BB temperatures. The VIIRS sensor was operated in diagnostic mode and each collect contains 100 scans. The sensor was set to fixed high gain.

2. Test Setup and Analysis

The LABB, OBC BB, and SVS were used as sources. The LABB was fixed at ~345 K, the OBC BB was fixed at ~310 K, and the SVS was near ambient (~294 K). The SVS was placed at ~55.5 degrees scan angle; the OBC BB was fixed at ~100 degrees scan angle.

The EV was rotated to start at -60.06 degrees scan angle, then a sector rotation was performed with a scan encoder delta of -910 (or -9.998 degrees). This placed the start of EV at -70.06 degrees scan angle, the SVS source was observed through the OBC BB collect window, and the OBC BB was observed through the SD collect window. The LABB was positioned from -65.7 to 35 degrees scan angle (as described in Table 1).

All samples were extracted for each collect for M12. A centroid of the LABB profile was determined for each collect (using only the samples with dn ≥ 100); this centroid was used to select the sample range listed in Table 1 (± 25 samples from the centroid). If a scan angle was repeated, then the average centroid was used. If the LABB profile was on the edge of the sample range, then the number of samples from the edge of the profile to the centroid from previous collects was used to determine the centroid from the observed side of the LABB profile.

The average OBC BB view data per scan was subtracted from all selected EV samples as well as all SD view samples. Then the EV and SD samples were averaged over their respective views, and finally averaged over all scans in a collect for each HAM side. The calibration view data used in this work was first truncated to 12 bits.

The HAM AOI for each collect was determined from the following [4]:

$$AOI = \cos^{-1}\left\{\cos 28.6 \cos\left[\frac{1}{2}(sample - 33.5)\frac{sample\_time}{scan\_rate}360 - \frac{1}{2}70.06 - 23\right]\right\} \tag{1}$$

where the middle selected sample was used here. The sample time was 88.26 μs and the scan rate was determined at each scan and averaged over the collect.

The at-detector radiance for the LABB and OBC BB sources can be expressed as [5]

$$\sum_{i=0}^{2} c_i dn^i_{LABB} = RVS_{LABB}\,\varepsilon_{LABB}\,L^{BB}_{LABB} - RVS_{SVS}\,L^{BB}_{SVS} - \frac{(RVS_{LABB} - RVS_{SVS})}{\rho_{RTA}}\left[L^{BB}_{HAM} - (1-\rho_{RTA})L^{BB}_{RTA}\right] \tag{2}$$

$$\sum_{i=0}^{2} c_i dn^i_{OBCBB} = RVS_{OBCBB}\,L_{OBCBB} - RVS_{SVS}\,L^{BB}_{SVS} - \frac{(RVS_{OBCBB} - RVS_{SVS})}{\rho_{RTA}}\left[L^{BB}_{HAM} - (1-\rho_{RTA})L^{BB}_{RTA}\right] \tag{3}$$

For the purposes of this test, the offset and nonlinear calibration coefficients were ignored and the ratio of the two above equations is (after rearranging)

$$\frac{RVS_{LABB}}{RVS_{OBCBB}} = \frac{\frac{dn_{LABB}}{dn_{OBCBB}}\left[L_{OBCBB} - \frac{RVS_{SVS}}{RVS_{OBCBB}}L^{BB}_{SVS} - \left(1 - \frac{RVS_{SVS}}{RVS_{OBCBB}}\right)\right] + \frac{RVS_{SVS}}{RVS_{OBCBB}}\left(L^{BB}_{SVS} - \frac{1}{\rho_{RTA}}\left[L^{BB}_{HAM} - (1-\rho_{RTA})L^{BB}_{RTA}\right]\right)}{L^{BB}_{LABB} - \frac{1}{\rho_{RTA}}\left[L^{BB}_{HAM} - (1-\rho_{RTA})L^{BB}_{RTA}\right]} \tag{4}$$

where

$$L_{OBCBB} = \varepsilon_{OBCBB}\,L^{BB}_{OBCBB} + (1-\varepsilon_{OBCBB})\left(L^{BB}_{SH} + L^{BB}_{CAV} + L^{BB}_{RTA}\right)/3 \tag{5}$$

Here L^{BB} refers to a spectrally weighted Planck radiance. Because both sides of Eq. (4) depend on the RVS, an iterative approach was used [3].

The RVS is then modeled as a quadratic polynomial in HAM AOI, or

$$RVS = a_0 + a_1 AOI + a_2 AOI^2 \tag{6}$$

The final RVS was then normalized to the SV HAM AOI (60.18 degrees).

The percent uncertainty is estimated by the following

$$u = 100\sqrt{\Delta^2_{fit} + \sigma^2_{fit}} \tag{7}$$

which is the RSS of the average fit residual and 1 sigma of the fit residual. This uncertainty accounts for the fitting and other statistical contributors; systematic uncertainty contributors have not been considered.

3. Results

Examples of the centroid determination are shown in Figures 1 and 2, using M12 data from UAIDs

4302126 and 4302127, respectively. Figure 1 shows the determination when the LABB profile is fully contained with the EV data. The vertical red line is the calculated centroid. Figure 2 shows a case when only part of the LABB profile was observed. The number of samples in Figure 1 from the edges of the profile to the centroid was used to determine the centroid in Figure 2 from the right side of the LABB profile.

The repeated RVS measurements at -8 degrees scan angle are plotted versus time in Figures 3 and 4 for all bands and detectors (HAM side A, subsample 1). The RVS is generally consistent over time, with the largest variation of about 0.4 % in M14. The MWIR bands tend to show less drift that the LWIR bands.

The relevant temperatures were extracted, and the Planck radiances calculated. Then the RVS in Eq. (4) was calculated for each collect. These RVS values were used to conduct a fit versus HAM AOI [as determined from Eq. (1)]. The measured RVS along with the fitted curves for all bands are shown in Figures 5 – 12, with HAM side A and B in the upper and lower plots, respectively. Note that the RVS in these plots is un-normalized. The MWIR show little dependence on HAM AOI, varying by less than 1 % across the full range of AOI. The LWIR show much greater variation, with M14 changing by ~10 % over AOI. In addition, very little HAM side or detector dependence was observed.

The final RVS for all bands [using detector 9 (17) for M (I) bands] is plotted in Figure 13, for HAM A and B. Here the RVS has been normalized to the SD angle (60.18 degrees HAM AOI). These results are consistent with VIIRS F1 measurements. The RVS fit coefficients are listed in Murphy charts, which are available upon request.

The uncertainty in the RVS [as defined in Eq. (7)], is shown in Figure 14. All bands are shown along the horizontal with detectors shown within a band from left to right. All bands, detectors, and HAM sides show uncertainties less than about 0.1 %. The red horizontal line is the general test requirement [1], 0.2 % for all bands except M14 (0.6 %).

4. Summary

FP-10 part 2 data was analyzed under ambient conditions for the VIIRS F2 sensor. RVS coefficients were determined for all thermal bands, detectors, and HAM sides. Analysis showed the following:

- The RVS variation across HAM AOI in the MWIR is small, on the order of 1 % or less. The LWIR RVS varies by between ~3 % (M16A and M16B) and ~10 % (M14).
- Detector dependence and HAM side dependence were observed to be small.
- Measured uncertainties are less than ~0.1 % for all bands.

Table 1: Data used in FP-10 part 2 analysis. Angles correspond to middle of sample range.

UAID	Collect	LABB Scan Angle	LABB HAM AOI	Samples Used	Collect Window
4302125	1	-8.87	38.81	1321-1674	2
4302126	1	-66.42	60.77	213-262	0
4302127	1	21.31	30.94	890-939	4
4302128	1	-45.88	52.37	1368-1417	0
4302129	1	5.21	34.62	1049-1098	3
4302130	1	-8.87	38.81	1321-1370	2
4302131	1	-56.27	56.57	784-833	0
4302132	1	-20.81	42.86	650-699	2
4302133	1	-38.79	49.58	703-752	1
4302134	1	-8.87	38.81	1321-1370	2
4302135	1	-51.73	54.72	1039-1088	0
4302136	1	34.38	29.14	1625-1674	4
4302137	1	-30.76	46.51	1154-1203	1
4302138	1	-8.87	38.81	1321-1370	2
4302139	1	-61.32	58.65	500-549	0
4302142	1	-61.32	58.65	500-549	0
4302145	1	-8.87	38.81	1321-1370	2
4302146	1	-8.87	38.81	1321-1370	2

Table 2: Sources temperatures [K] for FP-10 part 2 data.

UAID	Collect	LABB T	OBC BB T
4302125	1	345.0	310.9
4302126	1	345.0	310.9
4302127	1	345.0	310.9
4302128	1	345.0	310.9
4302129	1	345.0	310.9
4302130	1	345.0	310.9
4302131	1	345.0	310.9
4302132	1	345.0	310.9
4302133	1	345.0	310.9
4302134	1	345.0	310.9
4302135	1	345.0	310.9
4302136	1	345.0	310.9
4302137	1	345.0	310.9
4302138	1	345.0	310.9
4302139	1	345.0	310.9
4302142	1	345.0	310.9
4302145	1	345.0	310.9
4302146	1	345.0	310.9

Figure 1: Centroid determination for UAID 4302126 using M12 data.

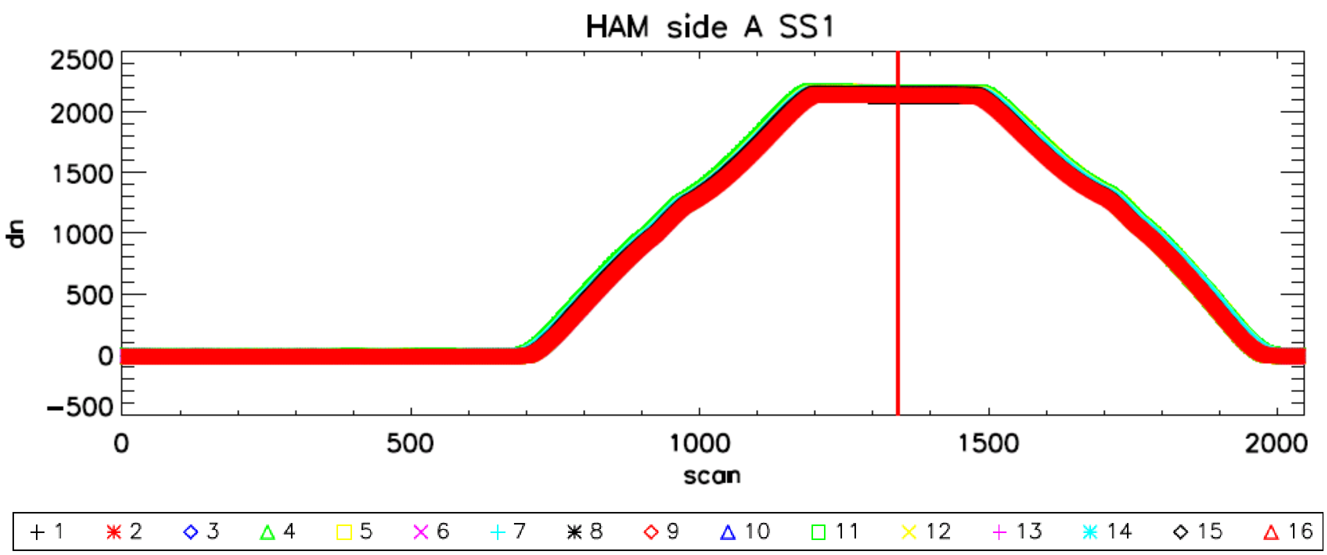

Figure 2: Centroid determination for UAID 4302127 using M12 data.

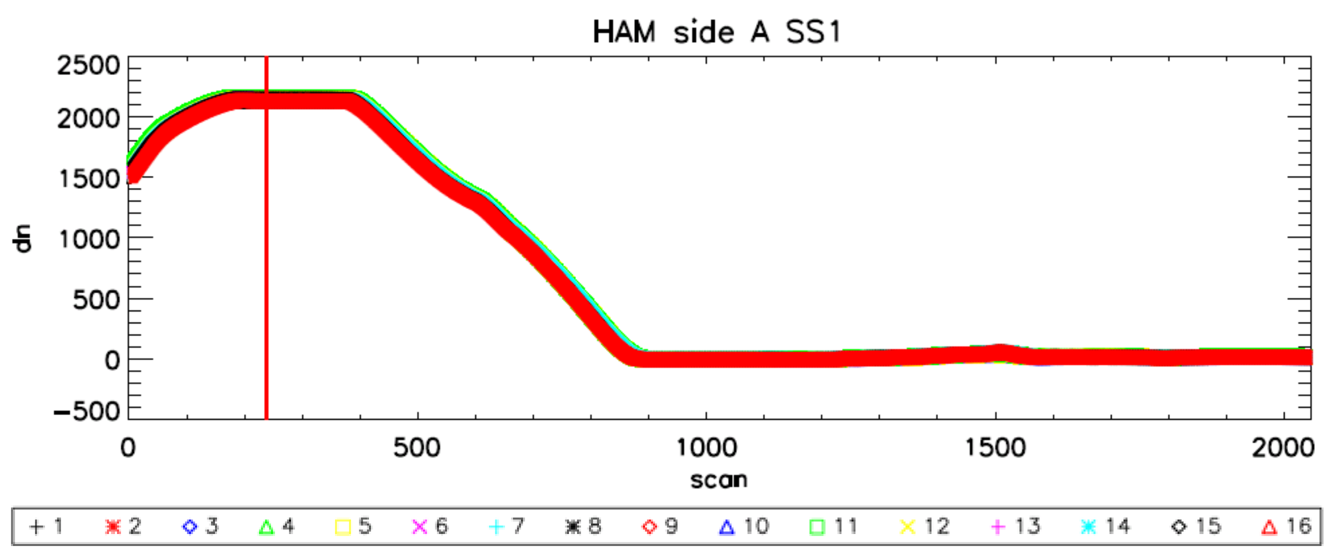

Figure 3: Repeated RVS measurements versus time at -8 degrees scan angle.

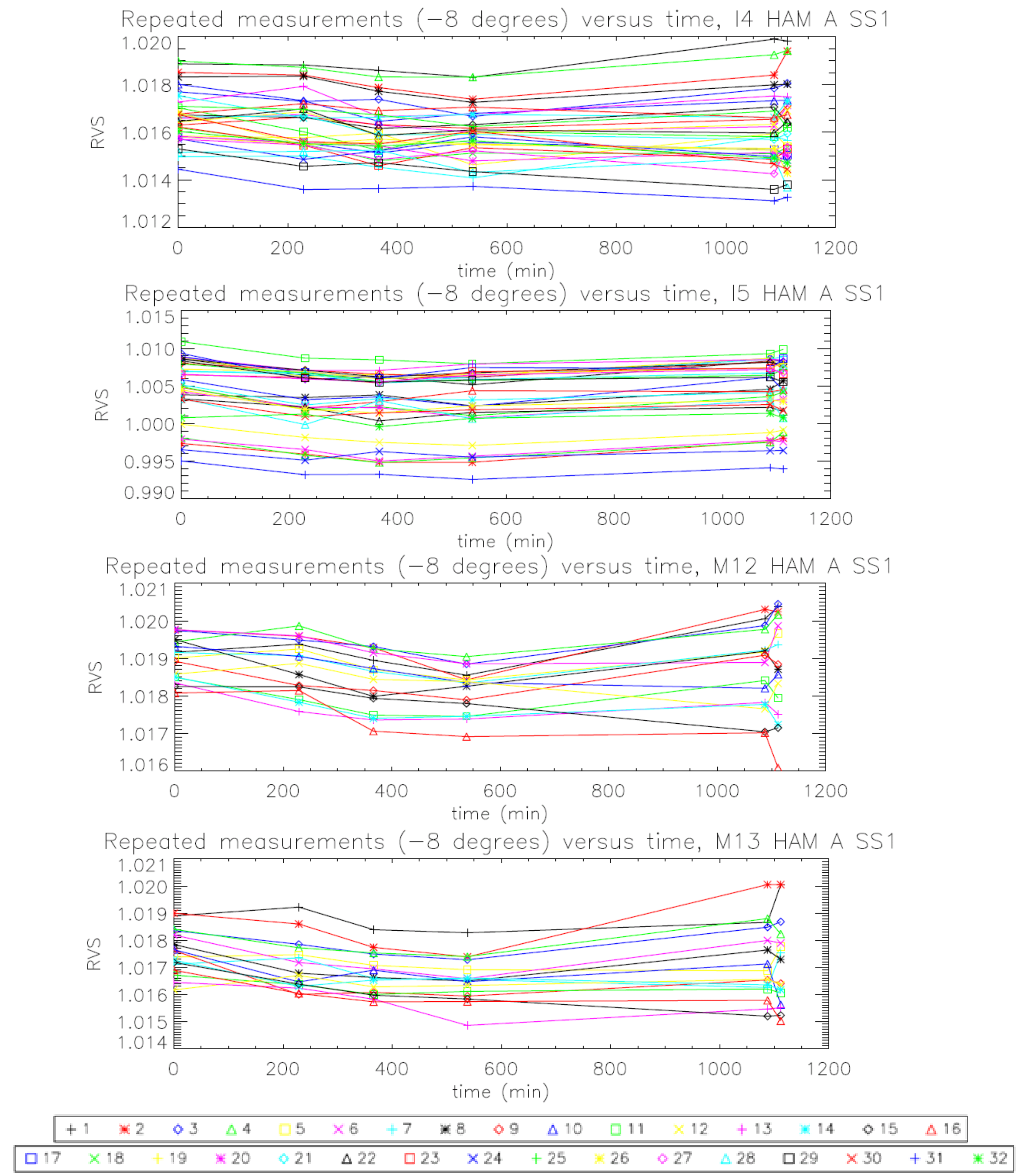

Figure 4: Repeated RVS measurements versus time at -8 degrees scan angle.

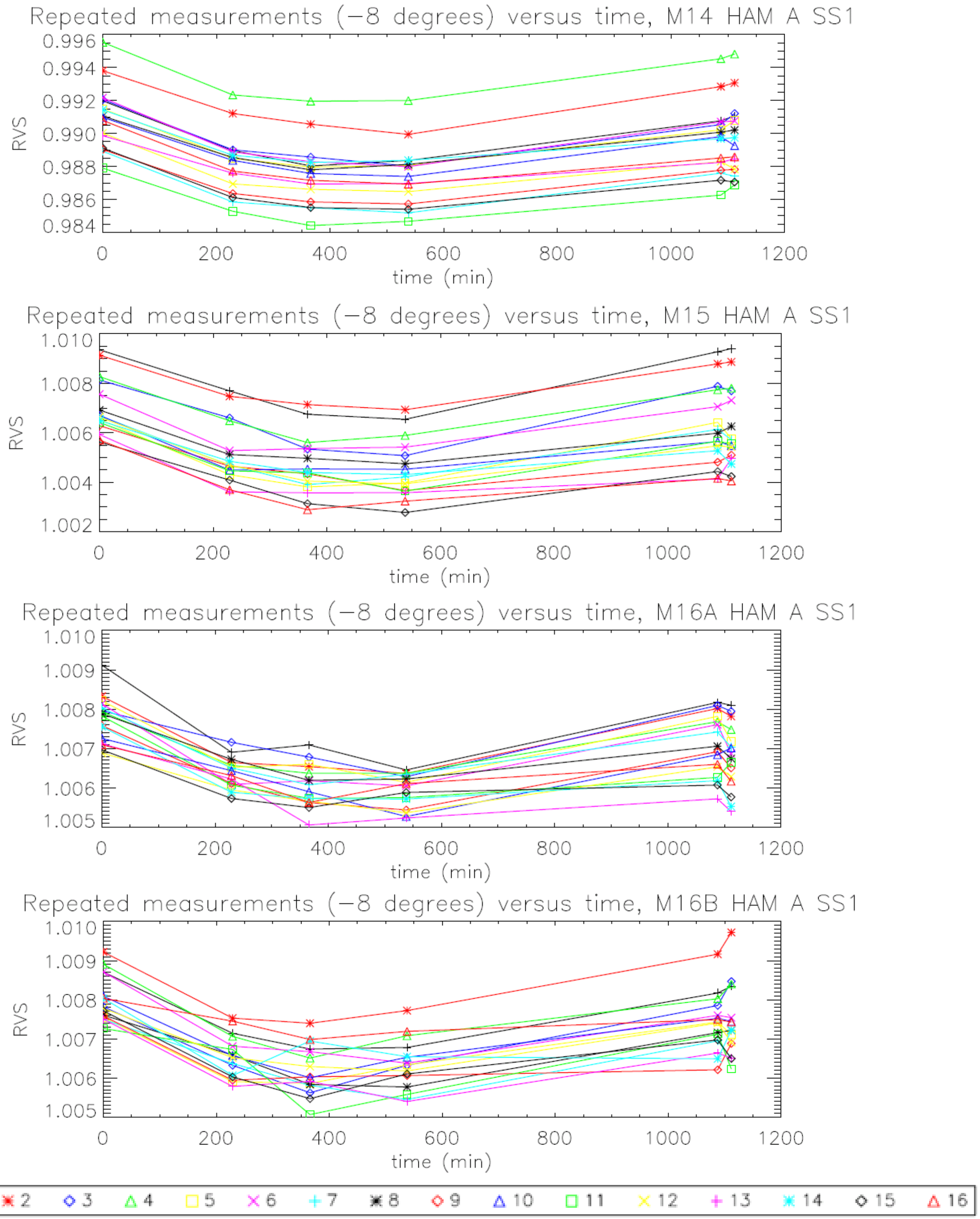

Figure 5: Measured (points) and fitted (lines) RVS for I4 SS1, HAM A (upper plot) and HAM B (lower plot).

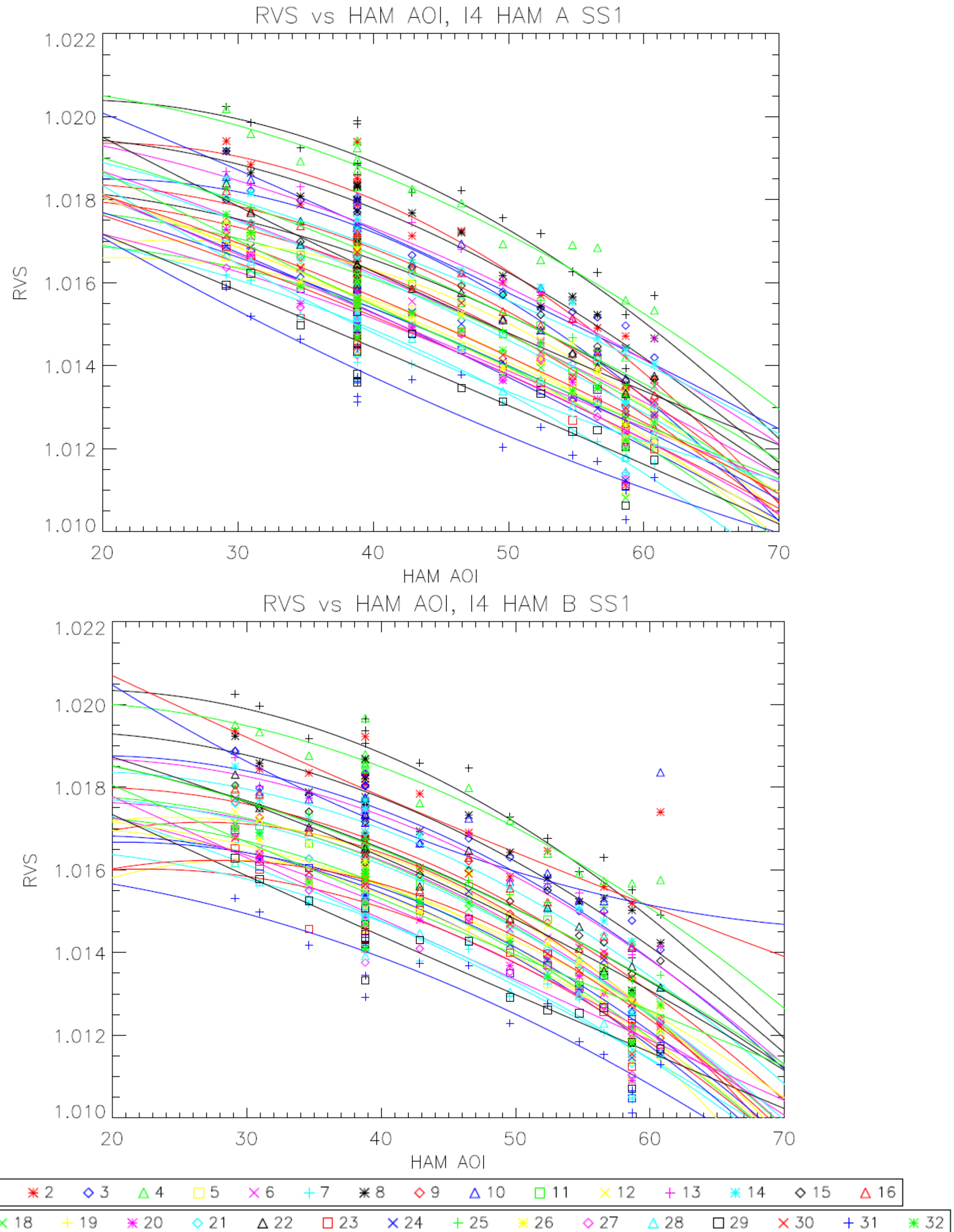

Figure 6: Measured (points) and fitted (lines) RVS for I5 SS1, HAM A (upper plot) and HAM B (lower plot).

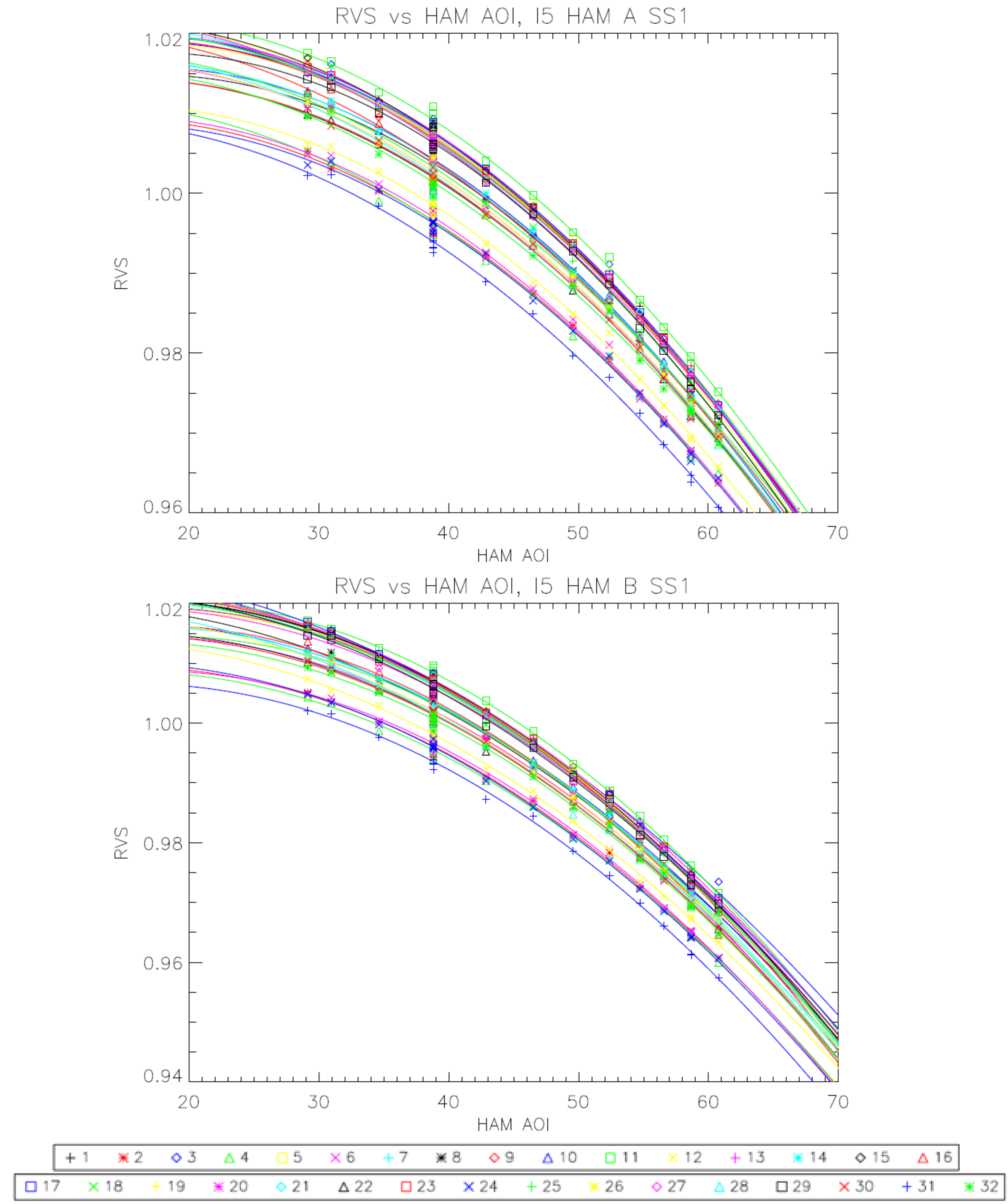

Figure 7: Measured (points) and fitted (lines) RVS for M12, HAM A (upper plot) and HAM B (lower plot).

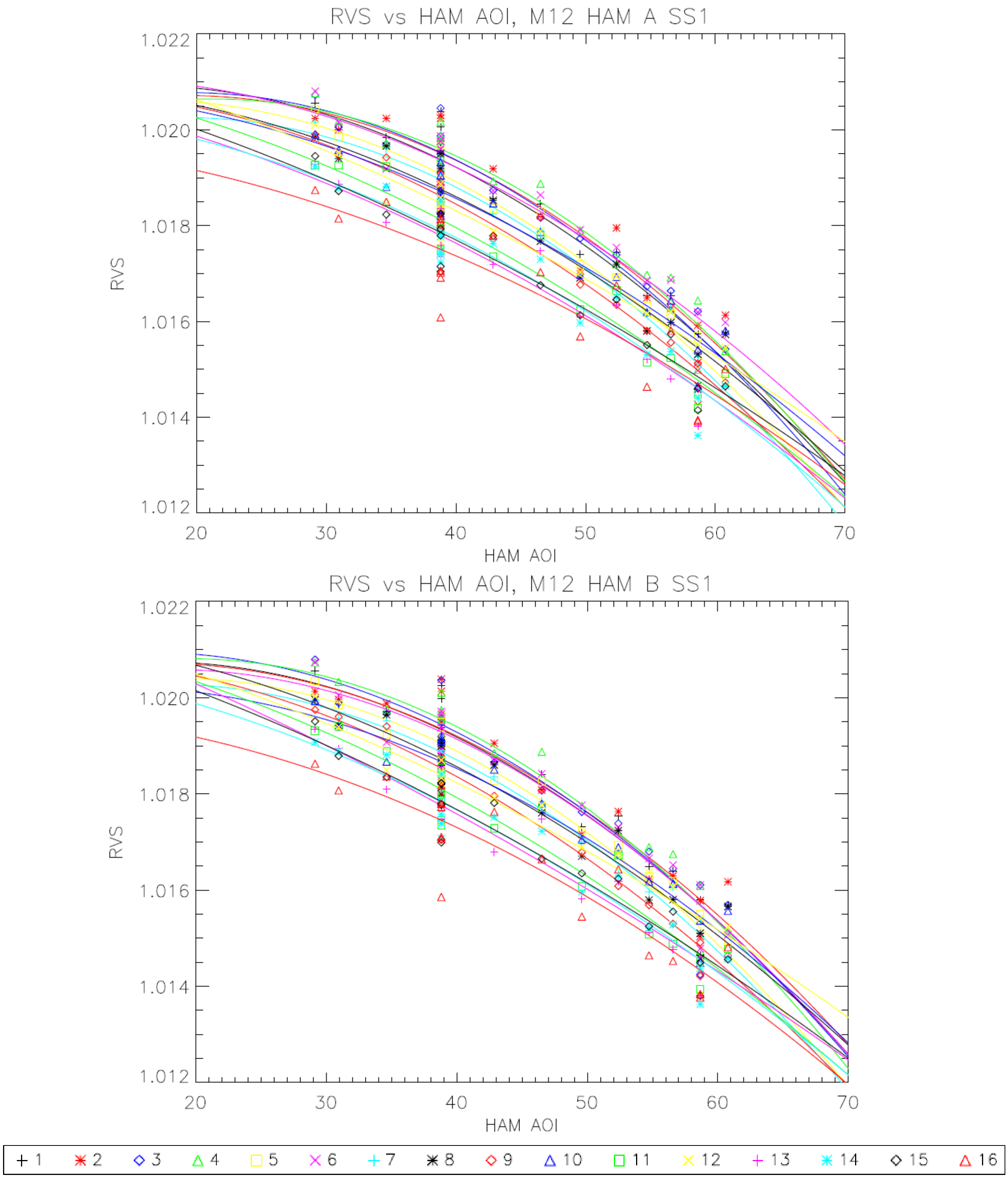

Figure 8: Measured (points) and fitted (lines) RVS for M13, HAM A (upper plot) and HAM B (lower plot).

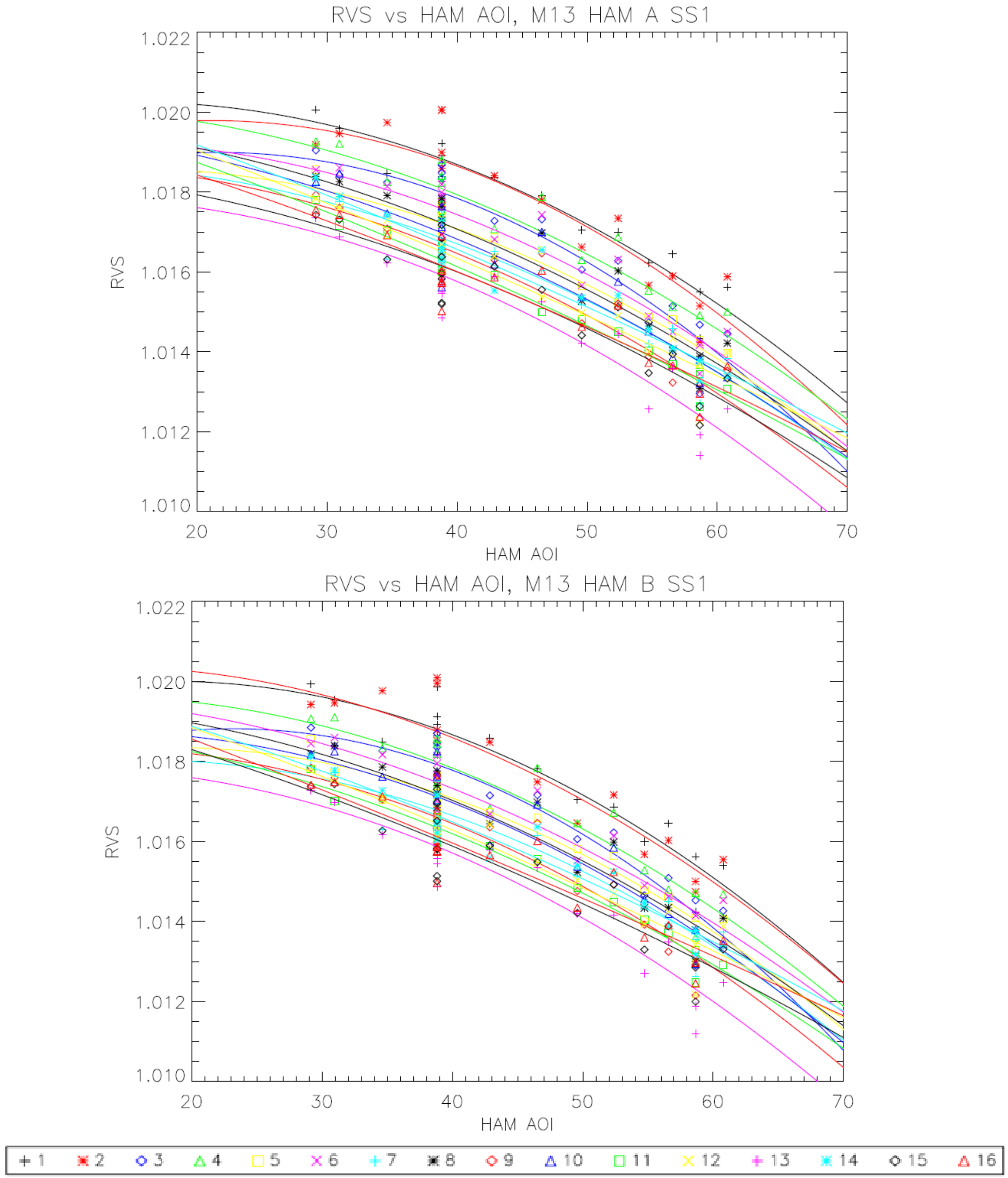

Figure 9: Measured (points) and fitted (lines) RVS for M14, HAM A (upper plot) and HAM B (lower plot).

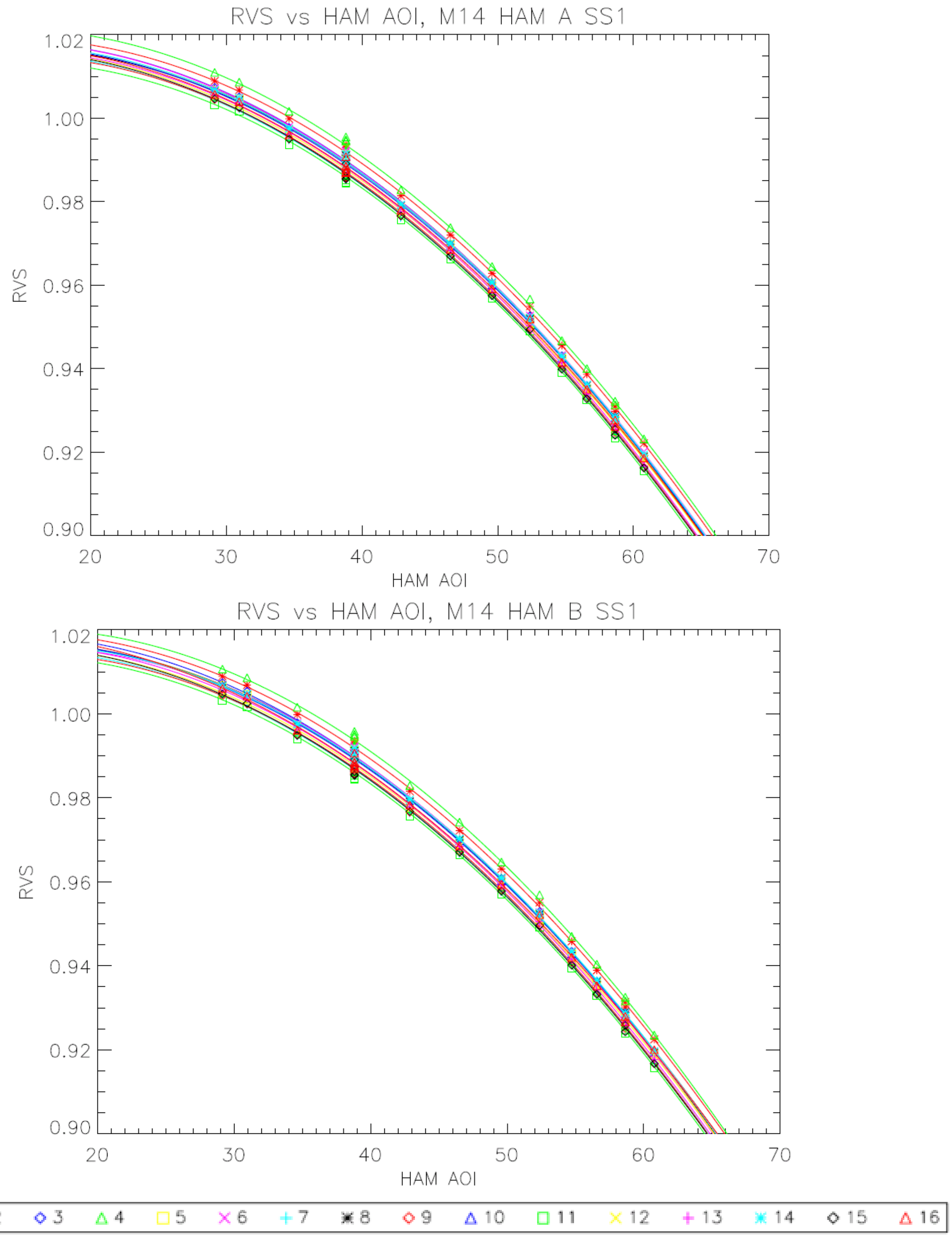

Figure 10: Measured (points) and fitted (lines) RVS for M15, HAM A (upper plot) and HAM B (lower plot).

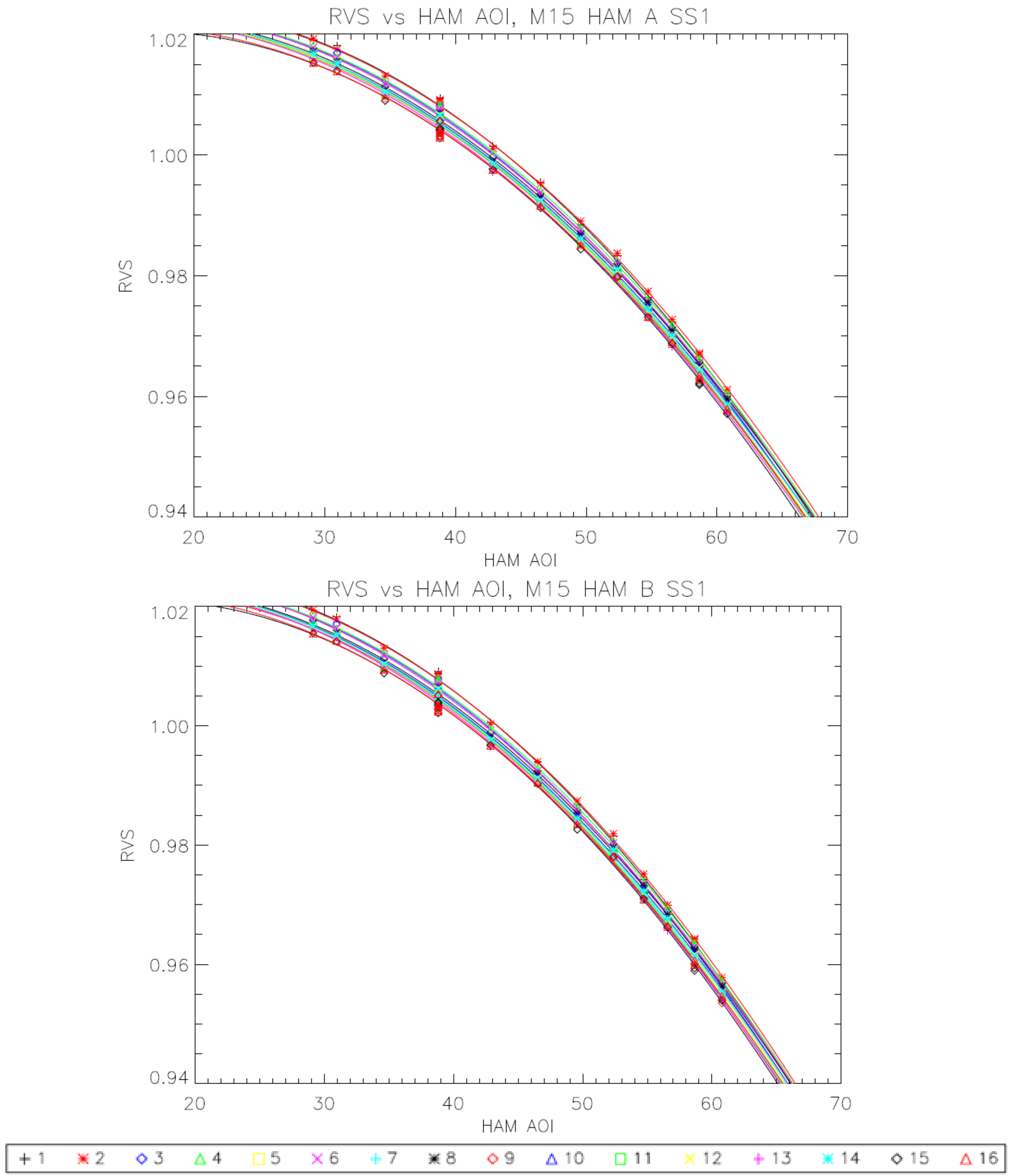

Figure 11: Measured (points) and fitted (lines) RVS for M16A, HAM A (upper plot) and HAM B (lower plot).

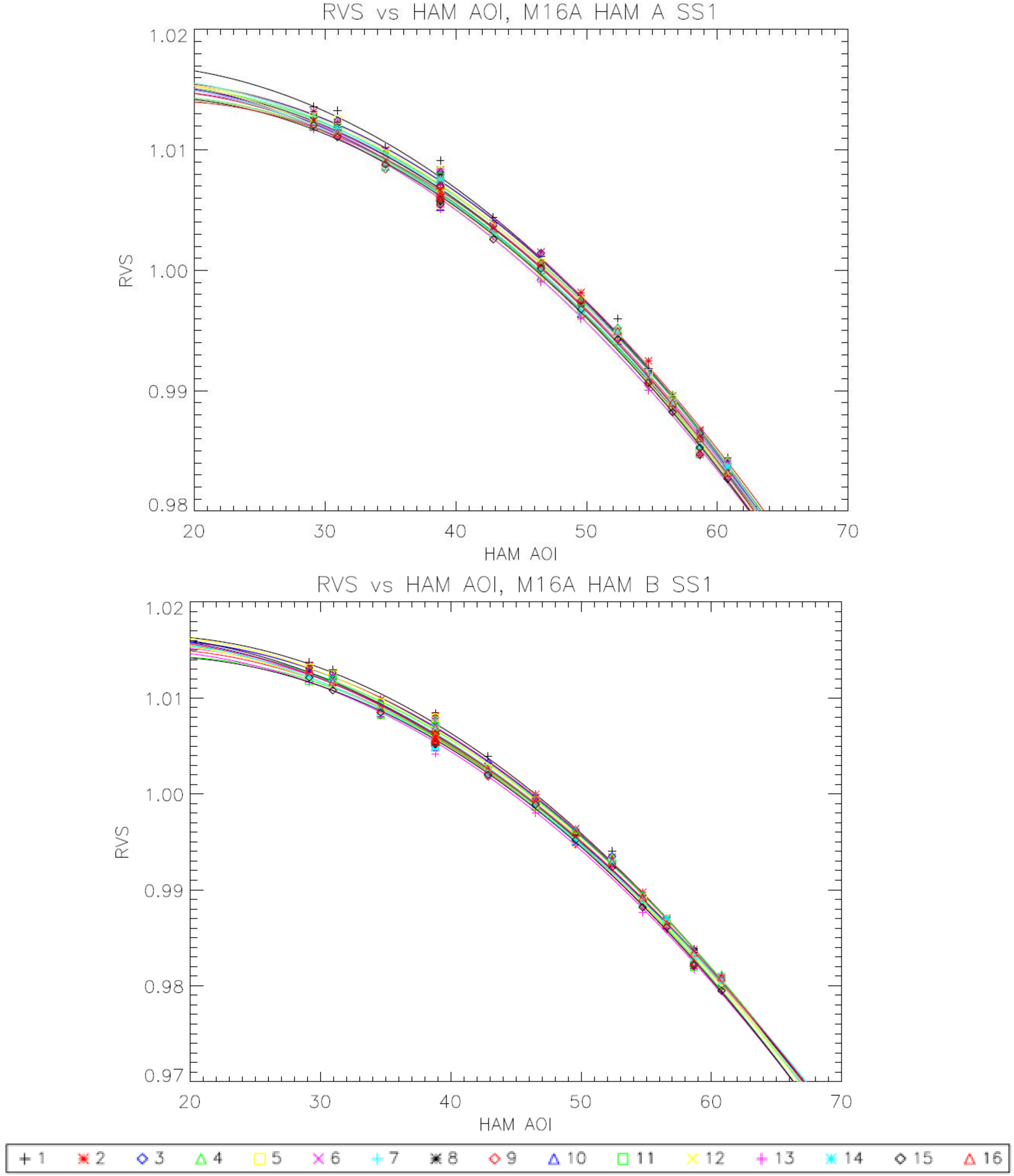

Figure 12: Measured (points) and fitted (lines) RVS for M16B, HAM A (upper plot) and HAM B (lower plot).

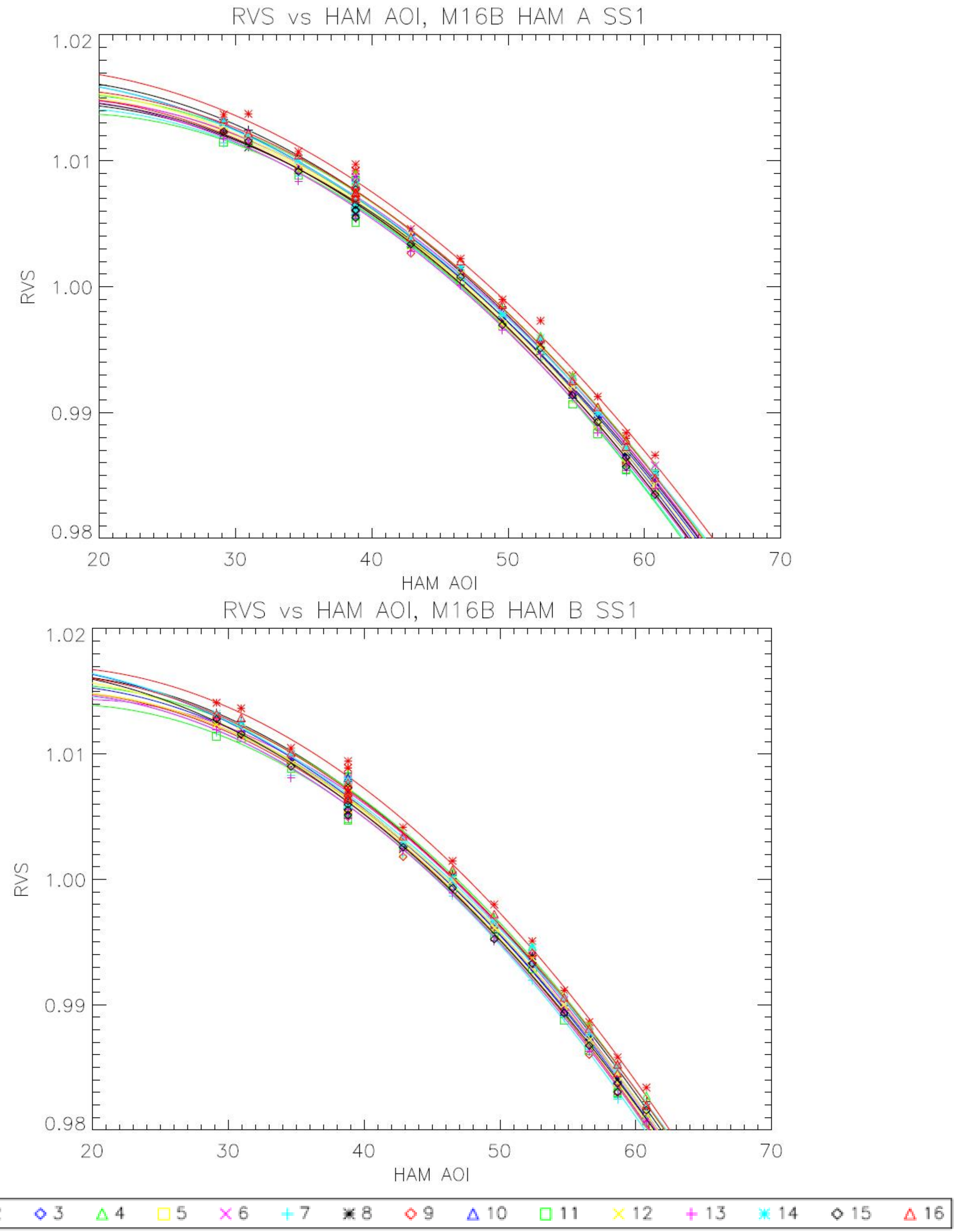

Figure 13: The final RVS for a middle detector for all bands and HAM A (upper plot) and B (lower plot),

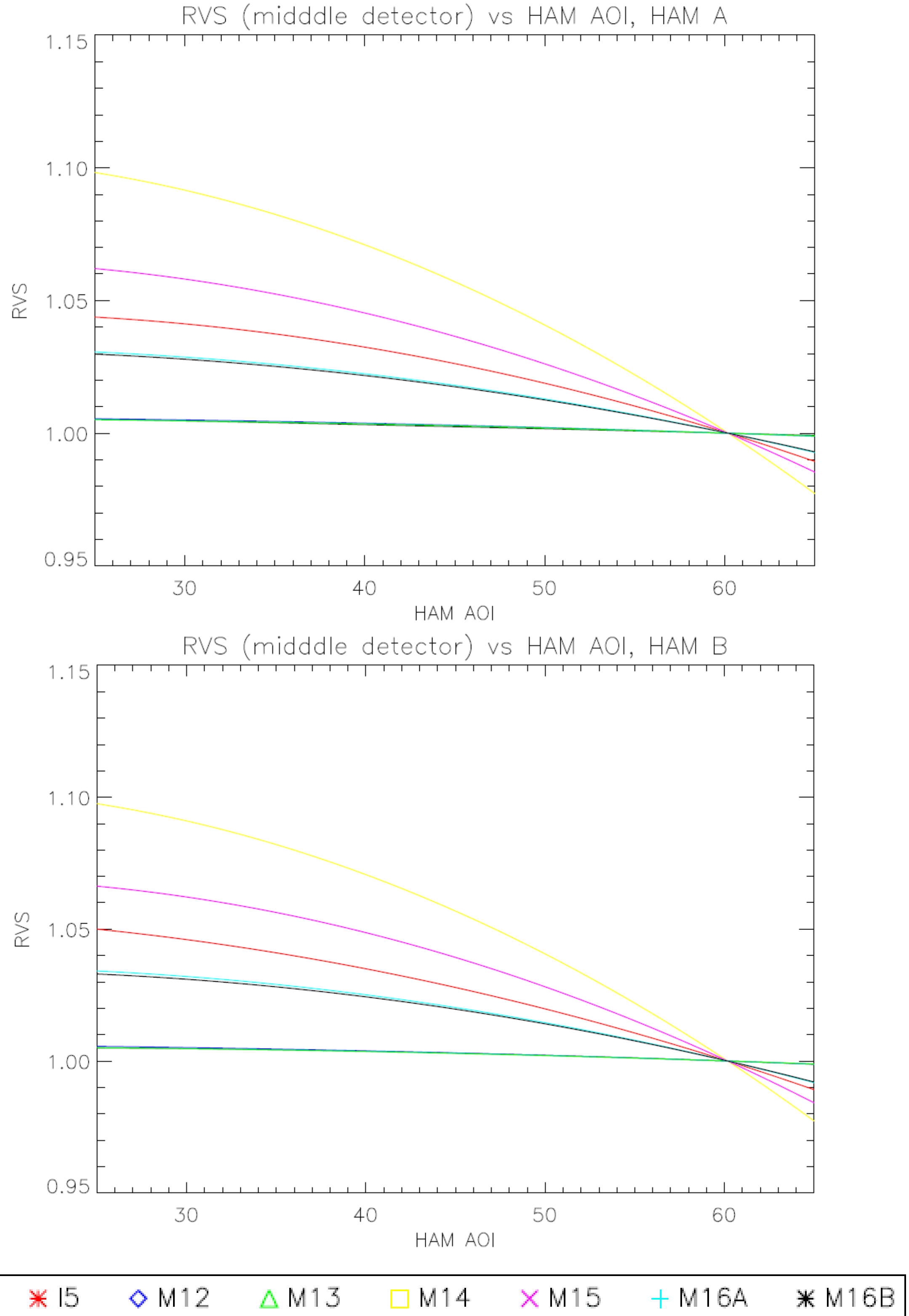

Figure 14: Uncertainty in RVS in [%].